11th World Congress on Computational Mechanics (WCCM XI)
5th European Conference on Computational Mechanics (ECCM V)
6th European Conference on Computational Fluid Dynamics (ECFD VI)
E. Oñate, J. Oliver and A. Huerta (Eds)

TOWARDS LARGE-EDDY SIMULATION OF COMPLEX FLOWS IN MARITIME APPLICATIONS

H.J. Bandringa[1*], R.W.C.P. Verstappen[1], F.W. Wubs[1], C.M. Klaij[2] and A. van der Ploeg[2]

[1] Faculty of Mathematics and Natural Sciences, University of Groningen (RUG), P.O. Box 800, 9700 AV, Groningen, The Netherlands, Email: h.j.bandringa@rug.nl - Web page: http://www.math.rug.nl/cmnm

[2] Maritime Research Institute Netherlands (MARIN), P.O. Box 28, 6700 AA Wageningen, The Netherlands, Email: info@marin.nl - Web page: http://www.marin.nl

Key words: Unstructured grid, LES model, Turbulence modelling, Circular cylinder

Abstract. Flows around bluff bodies, a circular cylinder for instance, are difficult to simulate accurately with a RANS method. To improve this type of simulations, LES models are considered in this paper. The idea behind these models is to minimize the subgrid dissipation. The models are based on the invariants of the rate of strain tensor. Also the governing equations are discretized such that less artificial dissipation is added. To proposed LES models are compared to an ILES model. The ILES model introduces artificial dissipation originating from the discretization of the governing equations. The comparison is performed using MARIN's in-house CFD solver ReFRESCO. A flow around a circular cylinder with $\mathrm{Re} = 3,900$ is considered here to evaluate the LES models. The (I)LES models clearly perform better than no model. The differences between the turbulence models, however, were small.

1 INTRODUCTION

Turbulent flows in maritime applications usually contain a wide range of length and time scales, especially for high Reynolds numbers. Therefore, it is not feasible to solve such flows with direct numerical simulation (DNS). To reduce CPU-times, turbulence models are used. However when considering a flow around a bluff body, like a circular cylinder, RANS models often do not provide the desired accuracy. Hence the focus in this paper is on LES models. In order to test several LES models, they have been implemented in MARIN's in-house CFD solver ReFRESCO. The finite volume code ReFRESCO can handle unstructured meshes, which is convenient for complex maritime applications with high Reynolds numbers. Additionally, local grid refinement can be applied to enhance the resolution in regions of interest.

This paper is organized as follows. In the first section the discretization of the Navier-Stokes equations will be discussed. The following section gives an overview of the LES models, which have been implemented in the CFD-solver ReFRESO. Then, numerical results for a flow around the circular cylinder with Re $= 3,900$ are presented. Results from an ILES model are also shown for comparison. This benchmark case has been studied many times, see for instances [1, 2, 3, 4, 5]. These references report small differences in the drag coefficient and the angle of flow separation, whereas the recirculation length shows much more spreading. Our results confirm this.

2 DISCRETIZATION OF NAVIER-STOKES EQUATIONS

The incompressible Navier-Stokes equations in integral form, for velocity component ϕ, are given by

$$\frac{\partial}{\partial t}\int_\Omega \rho\phi \mathrm{d}\Omega + \int_\Gamma \rho\phi(\mathbf{u}\cdot\mathbf{n})\mathrm{d}\Gamma + \int_\Gamma p\mathbf{n}\mathrm{d}\Gamma - \int_\Gamma (\mu\nabla\phi)\cdot\mathbf{n}\mathrm{d}\Gamma = 0, \qquad \int_\Gamma \mathbf{u}\cdot\mathbf{n}\ \mathrm{d}\Gamma = 0, \quad (1)$$

where Ω is any part of the fluid domain, $\Gamma = \partial\Omega$, ρ the density of the fluid, $\mathbf{u}$ the velocity vector. The dynamic viscosity is given by μ, p is the pressure.

The semi-discretized form of the incompressible Navier-Stokes equations becomes

$$\mathcal{M}\frac{d\mathbf{u}_h}{dt} + \mathcal{C}(\mathbf{u}_h)\mathbf{u}_h + \mathcal{G}p_h - \mathcal{V}\mathbf{u}_h = 0, \quad \mathcal{D}\mathbf{u}_h = 0, \quad (2)$$

where the diagonal mass matrix $\mathcal{M}$ is built from the volume of the fluid cells, $\mathbf{u}_h$ is the discrete velocity vector, $\mathcal{C}(\mathbf{u}_h)$ represents the discretization of the convective fluxes, $\mathcal{G}p_h$ is the discrete integrated pressure gradient, p_h is the discrete pressure, $\mathcal{V}(\mathbf{u}_h)$ represents the diffusive term and finally the discrete integrated divergence is denoted as $\mathcal{D}\mathbf{u}_h$.

The discrete variables, in ReFRESCO, are co-located at the cell centers, which is more convenient in combination with unstructured grids. The Navier-Stokes equations are solved implicitly in time by employing a second-order backward differentiation formula (BDF2)

$$\mathcal{M}\frac{3/2\mathbf{u}_h^{n+1} - 2\mathbf{u}_h^n + 1/2\mathbf{u}_h^{n-1}}{\Delta t} + \mathcal{C}(\mathbf{u}_h^{n+1})\mathbf{u}_h^{n+1} + \mathcal{G}p_h^{n+1} - \mathcal{V}\mathbf{u}_h^{n+1} = 0, \quad \mathcal{D}\mathbf{u}_h^{n+1} = 0. \quad (3)$$

The momentum equation is linearized by a Picard iteration. The linearized system of equations is solved using a SIMPLE algorithm [6].

2.1 Symmetry preserving discretization

Verstappen *et al.* [7] showed that if the discretization of the Navier-Stokes equations preserves the underlying symmetries no artificial damping is needed to stabilize the discretization, provided that the mesh stretching is mild. In order to obtain symmetry preserving discretization, the convection should be skew-symmetrically discretized,

$\mathcal{C}(\mathbf{u}_h) = -\mathcal{C}^T(\mathbf{u}_h)$, meaning a central scheme in which the face velocity is approximated by mesh-independent weights (e.g. $\phi_{ij} = \frac{1}{2}(\phi_i + \phi_j)$, where ϕ_{ij} is a value at the cell face between cell i and cell j). Also the transpose of the pressure gradient should be equal to minus the discrete divergence operator ($\mathcal{D} = -\mathcal{G}^T$). Since we have a cell centered grid arrangement, spurious pressure oscillations can occur. The approach in ReFRESCO is to employ the pressure weighted interpolation (PWI) method [8], which solves the pressure decoupling problem, but also introduces artificial dissipation [9]. Felten *et al.* [10] showed that the error (caused by the PWI) in the kinetic energy scales as $\mathcal{O}(\Delta t \Delta x^2)$. So by taking a small time step and a relative fine mesh, the error in the kinetic energy should be minimal.

2.2 Defect correction

A higher-order scheme such as QUICK leads to a wider stencil. On an unstructured grid where the Navier-Stokes equations are solved implicitly this is less desirable, since this wider stencil introduces more non-zero entries in the coefficient matrices $\mathcal{C}, \mathcal{G}$ and $\mathcal{V}$. The defect correction approach [11] (also called deferred correction) makes it possibles to use higher-order approximation without introducing a wider stencil. The higher-order approximations are calculated from a previous iteration and placed in the right-hand side of the linearized systems. A lower-order approximation will be put in the left-hand side and also in the right-hand side, where it is calculated from a previous iteration. For instance, the skew-symmetric discretized convection term is stated in defect correction form as

$$\mathcal{C}(\mathbf{u}_h)\mathbf{u}_h = \mathcal{C}(\mathbf{u}_h^k)_{\text{uds}}\mathbf{u}_h^k + \left(\mathcal{C}(\mathbf{u}_h^{k-1})_{\text{cds}}\mathbf{u}_h^{k-1} - \mathcal{C}(\mathbf{u}_h^{k-1})_{\text{uds}}\mathbf{u}_h^{k-1}\right), \tag{4}$$

where the subscript uds and cds stand for, respectively, upwind and central discretization. The k denotes here the current outerloop iteration (in which the non-linear Navier-Stokes equations are solved) and $k-1$ the previous outerloop iteration.

3 LARGE EDDY SIMULATION MODELS

For simulating flows around bluff bodies, RANS models may not be accurate enough. To improve the accuracy, LES models are appropriate, for instance. An LES model should resolve scales of size $\geq \Delta$, the filter length, whereas the scales smaller than Δ should be filtered out. In order to describe the interaction between the production of small scales of motion and the dissipation, the local strain tensor, $S(\mathbf{u}) = \frac{1}{2}\left(\nabla\mathbf{u} + (\nabla\mathbf{u})^T\right)$ (a real symmetric 3×3 matrix) is very useful [12]. The 2nd invariant and the 3rd invariant of the rate of strain tensor are given by

$$Q(\mathbf{u}) = \tfrac{1}{2}\text{tr}(S^2(\mathbf{u})), \tag{5}$$

$$R(\mathbf{u}) = -\tfrac{1}{3}\text{tr}(S^3(\mathbf{u})) = -\det\left(S(\mathbf{u})\right). \tag{6}$$

The quantity Q is a measure for the dissipation at the smallest scales. The transfer of energy from the resolved scales to the unresolved (subgrid) scales is represented by a

positive R, called forward scatter. If backscatter occurs ($R < 0$), the kinetic energy of subgrid scales is transferred back to the resolved scales. A proper LES model should include a proper treatment of forward scatter and backscatter.

3.1 Eddy viscosity model based on Q and R

The QR model, proposed by Verstappen [12] is formulated as

$$\frac{d}{dt}\int_\Omega \rho \mathbf{u}_\epsilon \mathrm{d}\Omega + \int_\Omega \rho(\mathbf{u}_\epsilon \cdot \nabla)\mathbf{u}_\epsilon \mathrm{d}\Omega + \int_\Omega \nabla p_e \mathrm{d}\Omega - \int_\Omega \nabla \cdot ((\mu + \mu_e)\nabla \mathbf{u}_\epsilon)\,\mathrm{d}\Omega = 0, \quad (7)$$

with the turbulent eddy viscosity, $\nu_e = \mu_e/\rho$, given by

$$\nu_e = \frac{3}{2}\frac{1}{\lambda_\Delta}\frac{|R|}{Q} \text{ or } \nu_e = \frac{3}{2}\frac{1}{\lambda_\Delta}\frac{\max(R,0)}{Q}, \quad (8)$$

where λ_Δ is the estimated smallest eigenvalue of the local discrete diffusion operator. The turbulent eddy viscosity is added at the locations where the small scales of motions are not resolved, to counteract the production term. In Eq. (8) two options are given for ν_e: $|R|$ and $R^+ = \max(R, 0)$. The former is active when forward scatter and backscatter occurs, while the latter is only active in the case of forward scatter and neglects the occurrence of backscatter.

Note that the classical Smagorinsky model reads $\nu_e = C_S^2\Delta^2\sqrt{4Q}$, with $C_S \approx 0.17$ and Δ a filter length. Since this model only incorporates Q, the Smagorinsky model is also active in regions where the flow becomes 2D or laminar. This is in constrast to the QR model, which is not active in that case since R becomes zero.

3.2 LES model based on regularization

To avoid interference with the subtle interplay between inertia and dissipation of the flow, artificial dissipation should be avoided. This can be accomplished by preserving the symmetries of the Navier-Stokes equations [7]. To restrain the production of small scales of motion, the convection term will be approximated by a regularization model, which smooths the convection using a filter operation. There is a whole class of regularization models [13], preserving the symmetries. Here, we consider the second-order approximation of the convection, $\mathcal{C}_2 = \overline{\mathcal{C}(\overline{u})\overline{u}}$. The filter F, defined by $F\phi = \overline{\phi}$, should be self-adjoint in order to keep the regularization model skew-symmetric. Trias *et al.* proposed to use a filter based on the Laplace operator, given by $F = (1 + \nabla \cdot (\alpha\nabla))$ [14]. The local variable parameter α which controls the filter is determined by a damping factor function f_2

$$f_2(\alpha) = \frac{\lambda_\Delta}{\rho/\mu}\frac{Q}{|R|}. \quad (9)$$

Note that filtering increases the complexity of the nonlinear system of equations, but by using a defect correction approach (see Section 2.2) the filtering does not enter into the matrix of the linear system.

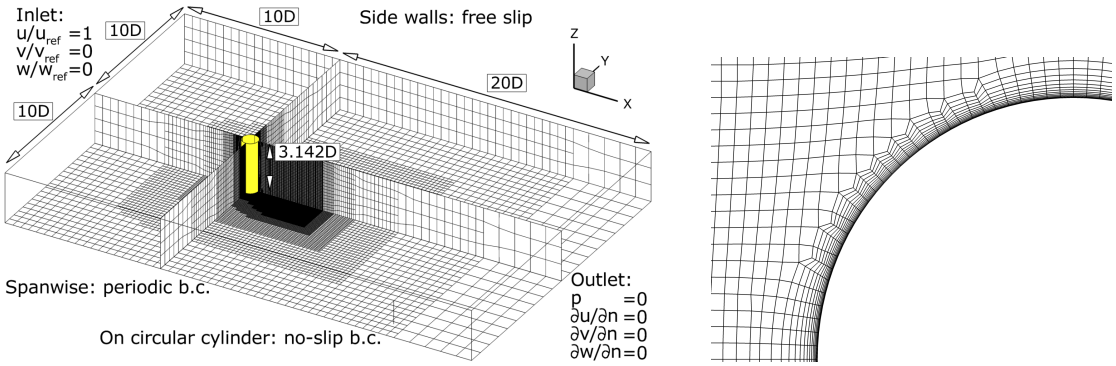

Figure 1: Overview of our numerical setup (*left*) and some mesh details of 0.84M grid (*right*).

3.3 Blend model

This model is a blend between an LES model based on regularization [13] and an eddy-viscosity model [12]. The non-linear convection term produces small scales of motion. At the smallest scale the diffusion should dissipate these scales. But on an LES grid, these smallest scales are not resolved. Therefore, an eddy viscosity will be computed such that the diffusion counteracts the production term. In order to prevent the transfer of energy from unresolved scales to resolved scales (backscatter), the convection term will be regularized.

Depending on the physics of the flow, the QR model or the regularization model will be used. If the energy is transferred from resolved scales to unresolved scales ($R > 0$), the QR model will be applied. A regularization model is imposed, when backscatter is appearing ($R < 0$).

4 CIRCULAR CYLINDER

The turbulence models will be tested for a turbulent flow around a circular cylinder with $\mathrm{Re} = \rho u_{ref} D/\mu = 3,900$, where D denotes the diameter of the cylinder. This benchmark case has been studied extensively, resulting in many numerical and experimental results, see for instance [1, 2, 3, 4, 5].

4.1 Setup numerical experiment

Our setup for the numerical experiments is displayed in Figure 1, where the description of the computational domain and the boundary conditions are shown. In this paper two meshes will be considered. The unstructured meshes, constructed with Hexpress [15], contain 0.20M and 0.84M grid cells. On the cylinder, in circumferential direction, 130 cells are situated for the 0.84M grid, whereas the coarser mesh only has 80 grid cells. This means that on the 0.20M grid every grid cell along the surface can only represent 4.5° and the finer mesh has at each 2.7° a grid cell. For both meshes, the mesh width perpendicular to the circular cylinder, defined as δ, is $1 \cdot 10^{-3}/D$. With this

δ the $y^+ = u_\tau y/\nu$ is at maximum 0.5, where u_τ is the friction velocity. Following the guidelines from Coleman *et al.* [16], our meshes satisfy the requirement that the first grid cell should be at $y^+ < 1$. Outside the boundary layer, in the near wake, the grid cells have size $h_x/D = h_y/D \approx 0.0313$ and $h_z/D \approx 0.0924$ for the 0.84M grid. The coarser mesh, 0.20M grid, has grid cells of size $h_x/D = h_y/D \approx 0.0521$ and $h_z/D \approx 0.175$. Some plots of the 0.84M mesh are shown in Figure 1. The dimensionless time step we took for all simulations was $\frac{u_{\text{ref}}\Delta t}{D} = 1/64$.

All the turbulence models, discussed in Section 3, will be tested here. Furthermore, results obtained with an Implicit LES model (a QUICK scheme with mesh-dependent weights and flux limiter) will be shown for comparison. Using an ILES model means that no subgrid scale model is implemented explicitly, instead the (locally) applied numerical dissipation suppresses the unresolved scales of motion. Also a central scheme with mesh-independent weights (see Section 2.1) without a turbulence model is considered here. Note that this will not be a DNS result, because the mesh is too coarse to capture all the small scales of motion. For the previous mentioned (turbulence) models a flux limiter is applied at a large distance of the cylinder ($x/D > 4.3$). At that location, the grid has less grid resolution, so the flux limiter will numerically damp out the flow, since we are not interested in that region.

4.2 Results

In Table 1 some global flow quantities are presented. Note that all of these quantities are averaged in time and span-wise direction. The lift and drag coefficients are nondimensionalized as follows $\mathrm{C}_D = \frac{F_x}{\frac{1}{2}\rho u_{ref}^2 LD}$ and $\mathrm{C}_L = \frac{F_y}{\frac{1}{2}\rho u_{ref}^2 LD}$, where F_x is the total force in the x-direction, consisting of the shear stress and the pressure acting in the x-direction. Here, $LD = 3.142D$ is the projected area of the circular cylinder. The total force in the y-direction is given by F_y, which consists of the normal stress and the pressure acting in the y-direction. The dimensionless Strouhal number is defined as $\mathrm{St} = \frac{\mathrm{f}_S D}{u_{\text{ref}}}$, where f_S is the frequency corresponding to the lift coefficient. The Strouhal number is determined from the spectra of the lift. l_r is the length of the recirculation zone. The angle at which the flow separates from the cylinder surface is denoted by ϕ_s, where 0° is located at the stagnation point and from there in clockwise direction it increases. Note that ϕ_s in our numerical experiments is determined by interpolation between two grid cells. Recall: on the 0.2M grid each grid cell represents 4.5°.

Before we start comparing our results with experimental measurements and numerical results from the literature, one remark has to be made. There is a large scattering in the mean flow results for the circular cylinder with $\mathrm{Re} = 3,900$ found in the literature, see Table 1 and Figure 2. Lehmkuhl *et al.* [2] observed that there are two modes present in the flow causing shrinking (mode H) and enlarging of the recirculation bubble (mode L). This phenomenon seems to be responsible for the large spreading in the mean flow results. In Table 1, one observes that the mean drag coefficient varies from 0.98 till 1.04. The

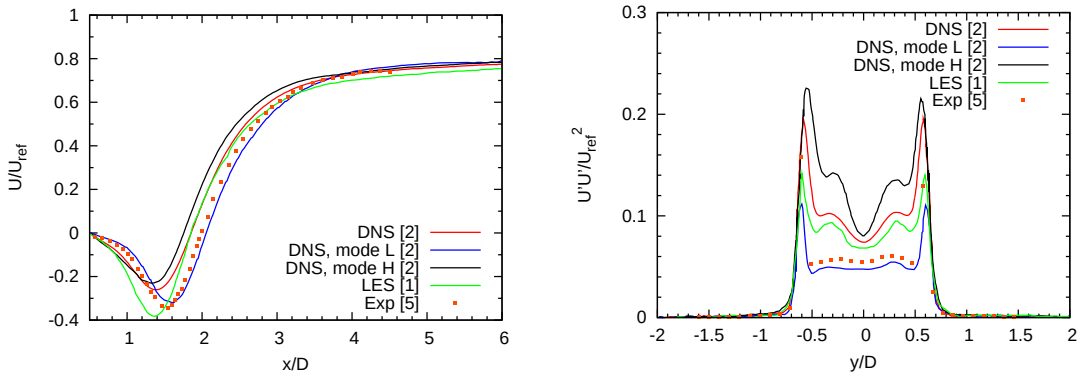

Figure 2: Example of large scattering of results found in the literature. *Left*: Time and span-wise averaged stream-wise velocity along the centerline. *Right*: Fluctuation of averaged steam-wise velocity at $x/D = 1.06$.

Strouhal number seems to be less dependent and is around 0.21. As already discussed the spreading in the length of the recirculation bubble is large. It goes from 1.26 till 1.66. The angle at which the flow separates from the cylinder surface is around 88°.

Table 1: Present numerical experiments compared with experimental measurements and numerical results from the literature.

	Mesh	Cycles	C_D	C_L	St	l_r	ϕ_s
No model (Central)	0.20M	13	1.127	0.003	0.202	0.88	91.7
ILES, QUICK with lim.	0.20M	28	1.211	0.004	0.211	0.78	91.2
QR with $\|R\|$	0.20M	35	1.113	0.004	0.202	1.04	90.9
QR with R^+	0.20M	35	1.122	0.010	0.200	0.98	91.2
C2	0.20M	20	1.014	-0.008	0.209	0.98	91.6
Blend	0.20M	28	1.038	-0.008	0.205	0.98	91.5
No model (Central)	0.84M	59	1.141	-0.001	0.211	1.39	88.5
ILES, QUICK with lim.	0.84M	88	1.017	-0.000	0.213	1.52	87.3
QR with $\|R\|$	0.84M	21	1.061	0.003	0.214	1.42	87.4
QR with R^+	0.84M	58	1.003	0.003	0.210	1.64	86.9
C2	0.84M	50	1.029	-0.001	0.218	1.23	88.1
Blend	0.84M	54	1.023	-0.002	0.217	1.30	87.9
Lehmkuhl *et al.* [2] (DNS)		850	1.015		0.215	1.36	88
Lehmkuhl *et al.* [2] (DNS, mode L)		250	0.979		0.218	1.55	87.8
Lehmkuhl *et al.* [2] (DNS, mode H)		250	1.043		0.214	1.26	88.25
Kravchenko *et al.* [1] (LES)		7	1.04		0.21	1.35	88
Norberg [3, 4] (Exp)			0.98		0.22	1.66	
Parnaudeau *et al.* [5] (Exp)		250			0.208	1.51	88

First we start comparing the global flow quantities from our numerical results on the 0.20M mesh with the reference data, reported in Table 1. First we observe that ϕ_s was not predicted at the correct location on the 0.20M grid. This is caused by the insufficient grid resolution to capture the geometry of the circular cylinder. Hence, the length of the recirculation zone is also incorrect for the 0.20M grid. The vortex shedding frequency or Strouhal number, however, seems to be correct. But despite this situation, (I)LES models and also the no-model simulation produce more or less the same results.

By looking at the results obtained on the 0.84M grid, it seems that most of the C_D's are within the range set by the results from the literature. Only the simulation without any model seems to predict a higher C_D. The C_L, although not reported in the literature, is almost zero for all models as it should be. The (I)LES models and simulation without any model predict the Strouhal number quite well, they are all in close agreement with the literature. The angle of flow separation is for almost all models less than 0.5° off compared to the reference data. Only the QR model with R^+ deviates with 1.0°. The length of the recirculation region, is however, very sensitive to mode L and H. This is also noticeable in our numerical results, because we do not have enough vortex shedding cycles compared to the reference data (see Table 1). Therefore, it may happen that the obtained results are closer to one of the modes instead of the long-time averaged results, where mode L or mode H are less pronounced. Therefore, we group our results, mainly based on the l_r, as well as possible and check if the results show similarities with the corresponding mode. Since the results on the 0.20M grid deviate a lot from our numerical results on the 0.84M grid and the reference data, the mean flow profiles are not shown here. Only for the 0.84M grid, some mean flow profiles are plotted in Figures 3-8. The fluctuations of the stream-wise velocity along the centerline Figures 3-5 show locally some wiggles. At those locations, the grid resolution makes a transition from fine to coarse with a factor of 2. This suddely decrease in cell size, in combination with the central scheme with mesh-independent weights, is causing this. The same phenomenon is also happening, although less noticeable, in the stream-wise velocity at $|y/D| > 1$, see Figures 6-8.

The turbulence models and the simulation without any model give varying results for the mean stream-wise velocity along the centerline, see Figures 3-5. The flow profiles, plotted in Figure 4, correspond well with the results from [2] and [5]. The associated fluctuations, however, seem to give a different profile than the ones obtained in the literature. The results in Figure 3 show that the stream-wise velocity as well as the fluctuations resemble also the reference data. Only the top of the fluctuations is somewhat lower than what is obtained in the literature. Also in Figure 5, the shape of the fluctuations is similar to the reference data, but again the top of the fluctuations obtained with the turbulence models is lower. The simulation without any model predicts a too high and too wide peak, which indicates that the no-model simulation has too little dissipation. The local minimum velocity in the recirculation bubble seems to be larger than what is found in the literature. Considering the stream-wise velocity at $x/D = 1.06$ and its corresponding

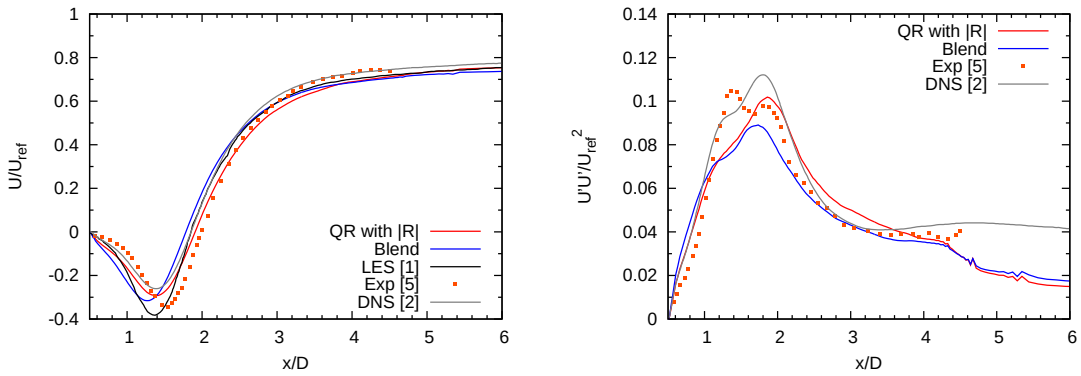

Figure 3: Time and span-wise averaged stream-wise velocity (*left*) and its fluctuation (*right*) along the centerline on the 0.84M grid. Results are compared with results from the literature, without a preference for mode L or H.

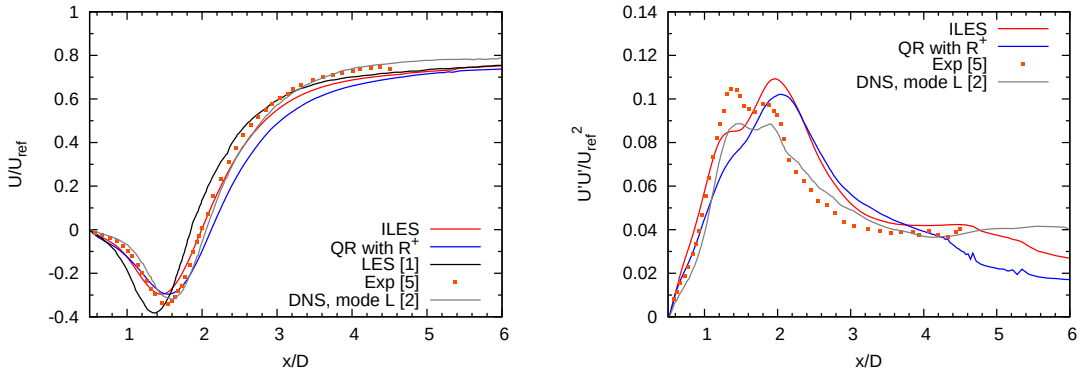

Figure 4: Time and span-wise averaged stream-wise velocity (*left*) and its fluctuation (*right*) along the centerline on the 0.84M grid. Results are compared with mode L results from the literature.

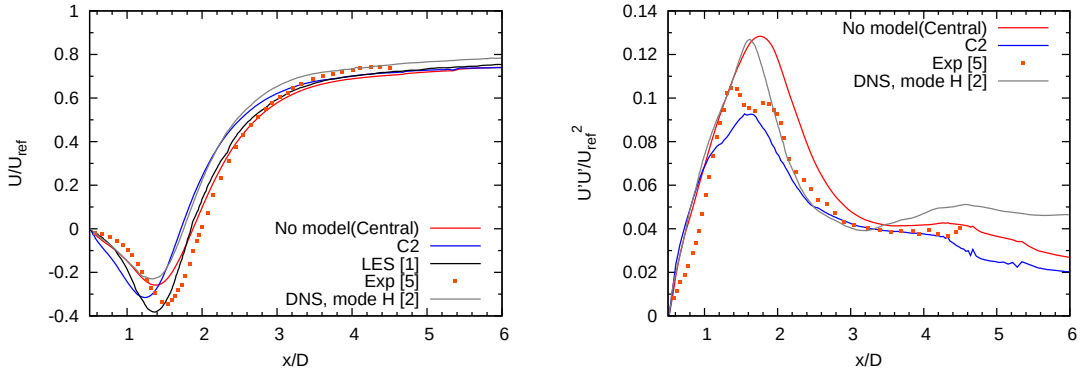

Figure 5: Time and span-wise averaged stream-wise velocity (*left*) and its fluctuation (*right*) along the centerline on the 0.84M grid. Results are compared with mode H results from the literature.

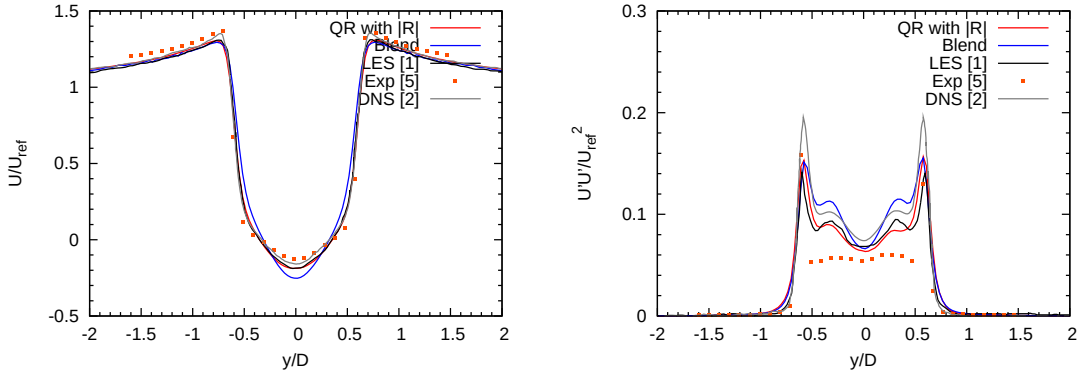

Figure 6: Time and span-wise averaged stream-wise velocity (*left*) and its corresponding fluctuation (*right*) along $x/D = 1.06$ on the 0.84M grid. Results are compared with results from the literature, without a preference for mode L or H.

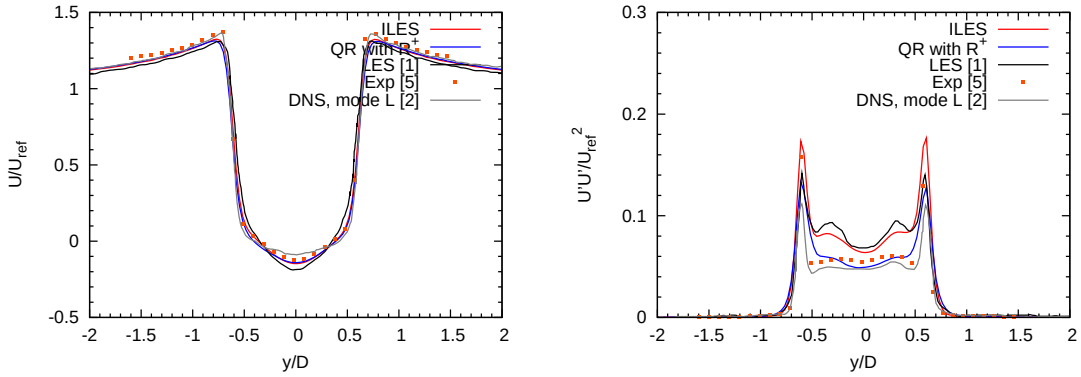

Figure 7: Time and span-wise averaged stream-wise velocity (*left*) and its corresponding fluctuation (*right*) along $x/D = 1.06$ on the 0.84M grid. Results are compared with mode L results from the literature.

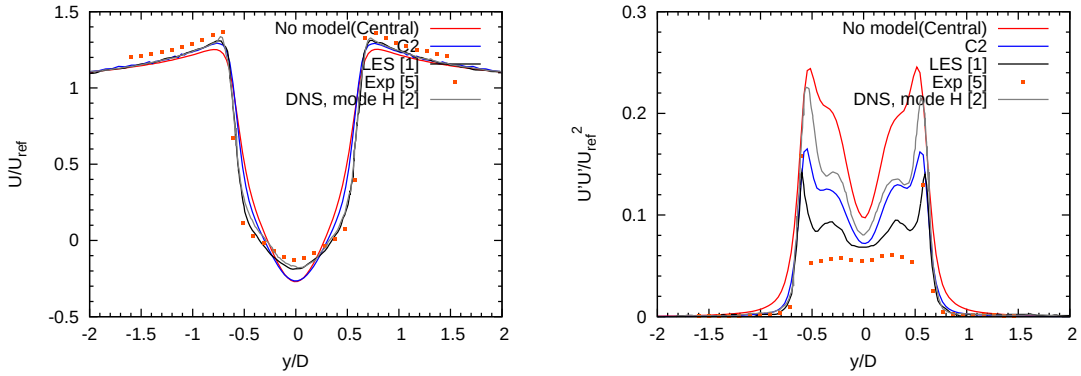

Figure 8: Time and span-wise averaged stream-wise velocity (*left*) and its corresponding fluctuation (*right*) along $x/D = 1.06$ on the 0.84M grid. Results are compared with mode H results from the literature.

fluctuation (Figures 6-8), the results obtained by the turbulence models predict globally the same flow profiles as given in the literature. The no-model simulation (Figure 8) predicts again a different profile.

5 CONCLUSIONS AND DISCUSSIONS

The novel LES models in combination with a symmetry preserving discretization, have been tested on a flow around a circular cylinder with $\mathrm{Re} = 3,900$. In order to investigate the differences of each of the proposed LES models, two meshes were considered. The coarsest mesh, containing 0.20M grid cells appears to be too coarse to capture the geometry of the circular cylinder. On this mesh, all of the proposed LES models and also the ILES model gave incorrect results. On the 0.84M grid, we observed two modes in the flow, just like Lehmkuhl *et al.* [2], which explains the large spreading in the global flow quantities and profiles we had in our numerical results. Therefore, we grouped the results for each of the (I)LES models and the simulation without any model based on the modes observed by Lehmkuhl et al. [2]. For each group, the turbulence models seem to give reasonable results. There was not really much difference between all of the (I)LES models. The simulation without any model, however, did not give satisfactory results, due to the lack of modelling the subgrid scales. To avoid the situation that we have to group our results, much more shedding cycles are needed. Roughly speaking, we need a factor 10 more, such that there is no preference anymore for a particular mode. So to summarize, even on a coarse mesh there was not much difference between the tested turbulence models and considering the fact that you need a lot of vortex shedding cycles, we concluded that the circular cylinder with $\mathrm{Re} = 3,900$ is not the most suitable test case for testing our proposed LES models. Therefore we will focus in the near future on a different test case, for instance a square cylinder with $\mathrm{Re} = 22,000$.

ACKNOWLEDGEMENT

The research reported in this paper is part of the project 'High-Quality Simulation of Complex Flows in Maritime Applications', which is part of the maritime innovation project (MIP) funded by Rijksdienst voor Ondernemend Nederland. This support is gratefully acknowledged.

REFERENCES

[1] A.G. Kravchenko and P. Moin, Numerical studies of flow over a circular cylinder at $Re_D = 3900$, *Phys. Fluids*, Vol. **12**(2):403-417, 2000.

[2] O. Lehmkuhl, I. Rodriguez, R. Borrell and A. Oliva. Low-frequency unsteadiness in the vortex formation region of a circular cylinder, *Phys. Fluids*, Vol. **27**(8): 1–21, 2013.

[3] C. Norberg, *Effects of Reynolds number and low-intensity freestream turbulence on the flow around a circular cylinder*, Tech. Rep. 87/2, Appl. Thermodyn. & Fluid

Mech., Chalmers Univ., Sweden, 1987.

[4] C. Norberg, LDV-measurements in the near wake of a circular cylinder, *Advances in Understanding of Bluff Body Wakes and Vortex-Induced Vibration*, Washington DC, 1998.

[5] P. Parnaudeau, J. Carlier, D. Heitz and E. Lamballais, Experimental and numerical studies of the flow over a circular cylinder at Reynolds number 3900, *Phys. Fluids*, Vol. **20**(8): 085101, 2008.

[6] C.M. Klaij and C. Vuik. SIMPLE-type preconditioners for cell-centered, colocated finite volume discretization of incompressible Reynolds-averaged Navier-Stokes equations. *Int. J. Numer. Meth. Fluids*, Vol. **70**(7), 830–849, 2013.

[7] R.W.C.P. Verstappen and A.E.P. Veldman. Symmetry-preserving discretization of turbulent flow. *J. Comput. Phys.*, Vol. **187**(1):343–368, 2003.

[8] T.F. Miller and F.W. Schmidt, Use of a pressure-weighted interpolation method for the solution of the incompressible Navier-Stokes equations on a nonstaggered grid system. *Numerical Heat Transfer*, Vol. **14**(2): 213–233, 1988.

[9] Shashank and J.L. Larsson and G. Iaccarino, A co-located incompressible Navier-Stokes solver with exact mass, momentum and kinetic energy conservation in the inviscid limit. *J. Comput. Phys.*, Vol. **229**(12): 4425–4430, 2010.

[10] F.N. Felten and T.S. Lund, Kinetic energy conservation issues associated with the collocated mesh scheme for incompressible flow. *J. Comput. Phys.*, Vol. **215**(2): 465–484, 2006.

[11] P. Wesseling, *Principles of Computational Fluid Dynamics*, 2001, Springer-Verlag, Berlin, Heidelberg

[12] R.W.C.P. Verstappen. When does eddy viscosity damp subfilter scales sufficiently? *J. Sci. Comput.*, Vol. **49**(1):94–110, 2011.

[13] R.W.C.P. Verstappen. On restraining the production of small scales of motion in a turbulent channel flow. *Comput. Fluids*, Vol. **37**(7):887–897, 2008..

[14] F.X. Trias and A. Gorobets and A. Olivia and C.D. Pérez-Segarra. DNS and regularization modeling of a turbulent differentially heated cavity of aspect ratio 5. *Int. J. Heat Mass Transfer*, Vol. **57**(1):171–182, 2013.

[15] http://www.numeca.com/en/products/automeshtm/hexpresstm

[16] G.N. Coleman and R.D. Sandberg, A primer on direct numerical simulation of turbulence - methods, procedures and guidelines. *Tech. Rep* AFM-09/01a. Aerodynamics & Flight Mechanics Research Group, School of Engineering Sciences, University of Southampton, Southampton, U.K.